AGU PUBLICATIONS

JGR

Journal of Geophysical Research: Solid Earth

RESEARCH ARTICLE
10.1002/2015JB011877

Key Points:
- Thermal convection in a contact aureole is simulated with a heat transfer model
- Organic maturation near a sill is used as a tracer of hydrothermal convection
- Observations match with permeability of at least a few tens of millidarcies

Supporting Information:
- Text S1 and Figures S1 and S2

Correspondence to:
D. Wang,
wangdy@dlut.edu.cn

Citation:
Wang, D., and M. Manga (2015), Organic matter maturation in the contact aureole of an igneous sill as a tracer of hydrothermal convection, *J. Geophys. Res. Solid Earth*, *120*, 4102–4112, doi:10.1002/2015JB011877.

Received 8 JAN 2015
Accepted 20 MAY 2015
Accepted article online 25 MAY 2015
Published online 19 JUN 2015

Organic matter maturation in the contact aureole of an igneous sill as a tracer of hydrothermal convection

Dayong Wang[1,2] and Michael Manga[2]

[1]Key Laboratory of Ocean Energy Utilization and Energy Conservation of Ministry of Education, School of Energy and Power Engineering, Dalian University of Technology, Dalian, China, [2]Department of Earth and Planetary Science, University of California, Berkeley, California, USA

Abstract The intrusion of magmas can induce hydrothermal convection which in turn enhances the transport of heat and solutes. We use a heat convection model to interpret the temperature evolution documented by organic matter maturation, as recorded by the vitrinite reflectance *Rr*, in a contact aureole of a 15 m thick basaltic sill in the Deep Sea Drilling Project (DSDP) 41–368 hole near Cape Verde Rise, eastern Atlantic. Here there is a pronounced asymmetry of variations of *Rr* with distance above and below the sill that cannot be explained by heat conduction alone. Neglecting the effects of possible two-phase flow and thermal pressurization from the production of fluids, convection begins to enhance the observed asymmetry for permeabilities greater than about 1 md, and the observations can be matched with permeabilities of at least several tens of millidarcies.

1. Introduction

Heat transferred from cooling igneous intrusions can drive hydrothermal circulation and thus enhance the transport of heat and solutes. This heat transport influences not only the contact aureole surrounding the intrusions but also the solidification history of the intrusions themselves. The maturation of organic matter in contact aureoles around intrusions can record this thermal history [*Bostick and Pawlewicz*, 1984; *Barker et al.*, 1998; *Stewart et al.*, 2005; *Wang et al.*, 2007; *Mastalerz et al.*, 2009; *Schimmelmann et al.*, 2009; *Vasquez et al.*, 2009; *Aarnes et al.*, 2010, 2011; *Valentim et al.*, 2011; *Cao et al.*, 2013].

Heat transfer models have been extensively used to assess the thermal effects of igneous intrusions on organic-rich host rocks and to relate intrusion to the petrology, geochemistry, and hydrocarbon generation potential [*Bishop and Abbott*, 1995; *Othman et al.*, 2001; *Jones et al.*, 2007; *Wang et al.*, 2008; *Santos et al.*, 2009; *Wang et al.*, 2010; *Wang and Song*, 2012; *Wang*, 2013; *Wang et al.*, 2013]. Most often, hydrothermal convection is assumed to be insignificant in low-permeability host rocks such as shale and mudstone [*Galushkin*, 1997; *Wang et al.*, 2007; *Fjeldskaar et al.*, 2008; *Aarnes et al.*, 2010]. However, asymmetric thermal alteration zones sometime occur around sill intrusions, implying that hydrothermal convection transports heat [e.g., *Galushkin*, 1997; *Wang et al.*, 2007]. Heat conduction models also suggest a greater thermal effect underneath intrusions than above in contradiction with inferences based on geothermometers [*Wang et al.*, 2011a, 2011b; *Wang and Song*, 2012].

Here we use two-dimensional numerical simulations of the effects of hydrothermal convection on organic matter maturation adjacent to an igneous sill to interpret measurements from a well-characterized intrusive sill. By comparing model predictions to measurements, we can reconstruct the thermal evolution of the contact aureole. We find that the observed asymmetry in maturation can be explained by reasonable values of permeability.

2. Geological Example

A 15 m thick basaltic sill in the Deep Sea Drilling Project (DSDP) 41–368 hole (17°30.4′N, 21°21.2′W) near the Cape Verde Rise, eastern Atlantic, is selected as a geological example. The sill horizontally intruded into shale strata (Figure 1) [*Simoneit et al.*, 1978; *Galushkin*, 1997]. Due to the shallow burial depth below the seafloor (~956 m below sea level (bsl) at present and 780 m bsl at the time of emplacement 19 Ma), the porosity of host rocks is high, approximately 0.4 [*Lancelot and Seibold*, 1977; *Galushkin*, 1997]. More detailed information about this sill and its setting is provided by *Peters et al.* [1983], *Galushkin* [1997], and *Wang et al.* [2011a, 2011b],

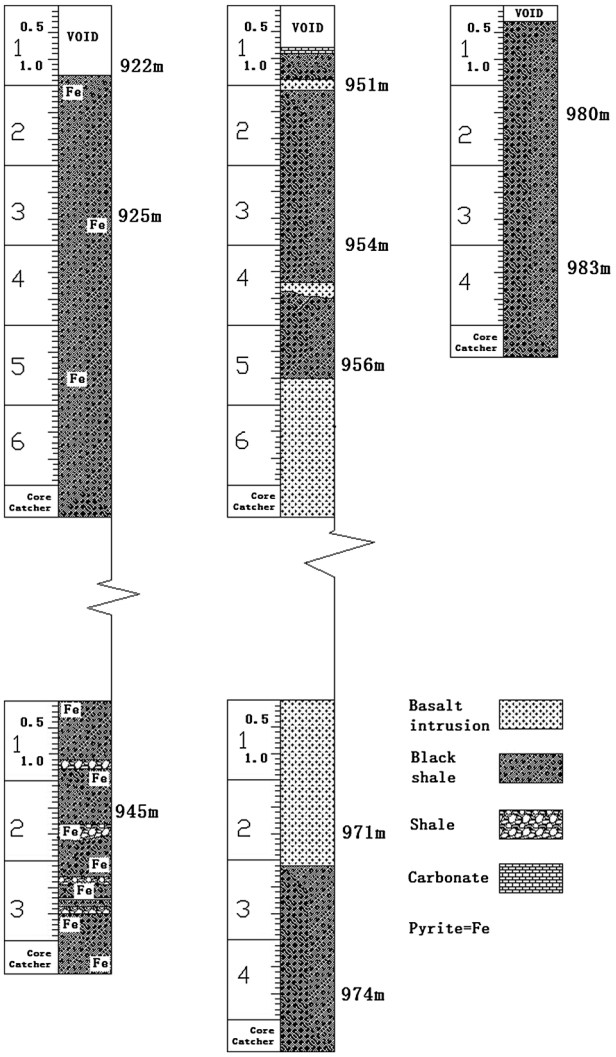

Figure 1. The lithology log in the vicinity of the 15 m thick basaltic sill (modified from *Simoneit et al.* [1978]).

in particular, thermophysical properties of the sill and the host rocks [*Galushkin*, 1997; *Wang et al.*, 2011a, 2011b], total organic carbon contents (Figure 2) [*Simoneit et al.*, 1981], and thermal evolution of the host rocks before intrusion of magma [*Galushkin*, 1997].

Peters et al. [1983] measured vitrinite reflectance, *R*r over a depth interval of 924.8 to 983.4 m from core recovered by the Deep Sea Drilling Project, hole DSDP 41–368. Approximately 100 vitrinite particles were measured for each sample, and the moderate values were used (Figure 3) [*Peters et al.*, 1983]. The uncertainties in the measured *R*r are not provided in the original publications. Thus, we rely on other studies to infer reasonable uncertainties in the *R*r measurements. According to *Barker* [1996], the standard deviation (SD) of random *R*r measurements increases with the increase of *R*r. For a high *R*r value (e.g., 3.2%), the SD is ~0.30%, whereas for lower values (<2.0%), the SD is generally less than 0.2%. Thus, the uncertainty for the used *R*r values can be deduced to lie in a range of ±10% of the plotted values. Such uncertainties are also consistent with those previously reported by *Peters et al.* [1978]: the measurement uncertainty generally lies in a range of ±0.3% and is not higher than ±0.4%.

As shown in Figure 3, the *R*r profiles of the host rocks are asymmetric relative to the center of the sill: at the same distance from sill margins, the *R*r of the overlying host rocks is generally higher than that of the underlying host rocks, implying that the sill exerted stronger thermal effects on the overlying host rocks [*Galushkin*, 1997]. The thermal evolution of the host rocks was reconstructed by different types of one-dimensional heat transfer models [*Galushkin*, 1997; *Wang et al.*, 2011a, 2011b]; the importance of thermal convection of pore water in the thermal evolution of the host rocks remains disputed [*Galushkin*, 1997; *Wang et al.*, 2011a, 2011b], motivating the present study.

3. Methods

3.1. Modeling Heat Transfer From the Sill to the Host Rocks

Some general assumptions are required to model heat transfer from a sill to its host rocks.

1. The shape of the intrusion is regular, reasonable for most dike- or sill-like bodies [*Jaeger*, 1959; *Turcotte and Schubert*, 1982; *Galushkin*, 1997; *Barker et al.*, 1998; *Stewart et al.*, 2005; *Wang et al.*, 2007; *Santos et al.*, 2009].
2. If the sill is just a few meters thick, 15 m in our example, convection in the magma can be ignored [*Jaeger*, 1959; *Galushkin*, 1997; *Fu et al.*, 2010; *Wang et al.*, 2011a, 2011b].
3. Heat removed by escaping nonwater volatiles can be neglected [e.g., *Jaeger*, 1959; *Barker et al.*, 1998; *Galushkin*, 1997; *Wang et al.*, 2007, 2011a, 2011b]. Since the effects of volatiles are dispersed over a region

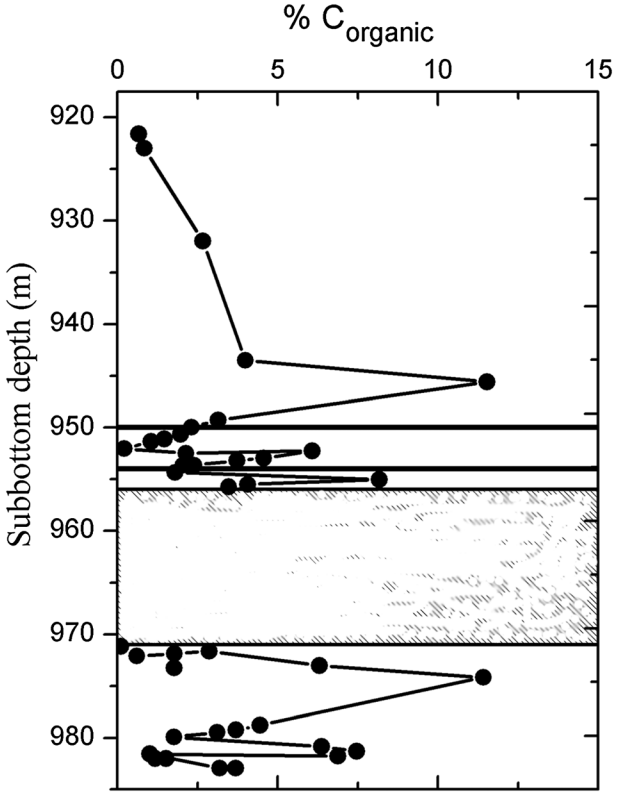

Figure 2. Total organic carbon content above and below the large sill (modified from *Simoneit et al.* [1981]).

whose thickness is many times that of the igneous sheet, it is reasonable to assume that the heat conveyed by them is also dispersed over a large region and thus will make little contribution to the temperature in the contact aureole.

4. We consider an isotropic, homogeneous porous medium. Figure 1 shows that the host rocks are mainly composed of shales. Because they still have a high porosity, we assume that they are a homogeneous porous medium with flow and heat transport occurring primarily through pore space rather than fractures. Assuming that the host rocks are anisotropic and heterogeneous will significantly complicate the interpretation of model results. We thus make the same assumptions as typically done [e.g., *Hanson*, 1995; *Norton and Hulen*, 2001; *Iyer et al.*, 2013].
5. Thermal pressurization caused by fluid production and the transient changes in porosity occur shortly after magma emplacement [*Delaney*, 1982], but because it occurs over very short time scales, it is usually neglected in models [e.g., *Galushkin*, 1997; *Dutrow et al.*, 2001; *Norton and Hulen*, 2001]. Thus, the driving mechanism for fluid flow will be the thermal buoyancy of pore water.
6. We do not consider vapor-liquid two-phase flow [*Hayba and Ingebritsen*, 1997; *Dutrow et al.*, 2001]. Even if the pressure is hydrostatic (the lowest possible value), the pressure of pore fluids in the host rocks exceeds the critical pressure (22.1 MPa) of water at the burial depth of >4 km (water depth of 3367 m and 780 m bsl emplacement depth). Thus, a vapor phase is not expected at such pressures [*Jamtveit et al.*, 2004].

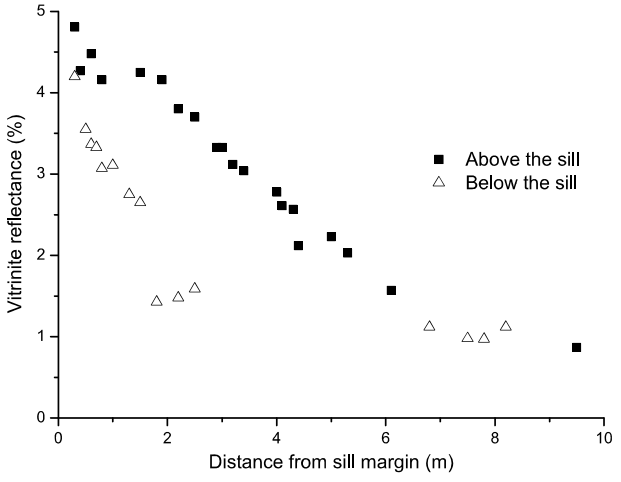

Figure 3. Vitrinite reflectance measured above and below a 15 m thick igneous sill [*Peters et al.*, 1983].

With these assumptions we solve a set of equations for heat and mass transport. Variables used in the equations are defined in Table 1. For the sill,

$$\nabla\cdot\left(K_{\text{magma}}\cdot\nabla T\right) + \frac{H_1}{T_{C1}-T_{C2}}\cdot\frac{\partial\left(\rho_{\text{magma}}\cdot T\right)}{\partial t} = \frac{\partial\left(\rho_{\text{magma}}\cdot C_{\text{magma}}\cdot T\right)}{\partial t} \quad . \tag{1}$$

For the host rocks,

$$\nabla\cdot(K_{\text{host}}\cdot\nabla T) - (\rho_{\text{water}}\cdot C_{\text{water}}\cdot\mathbf{u}\cdot\nabla T) + Q = \frac{\partial(\rho_{\text{host}}\cdot C_{\text{host}}\cdot T)}{\partial t} \quad . \tag{2}$$

Enthalpy of mineral dehydration is much larger than that of organic cracking [*Aarnes et al.*, 2010]. Thus, only the latent

Table 1. Basic Parameters for Two-Dimensional Heat Convection Models

Symbol	Value	Definition and Reference
A		The Arrhenius or frequency factor
C_{host}		The specific heat of host rocks
C_{magma}	1213 J kg^{-1}°C^{-1}	The specific heat of intrusive sill [*Galushkin*, 1997]
C_{matrix}	820 J kg^{-1}°C^{-1}	The specific heat of rock matrix of host rocks
C_{water}	4200 J kg^{-1}°C^{-1}	The specific heat of water
E_i		The activation energy for the *i*th reaction
f_i		The weight for the *i*th reaction
F		Transformation ratio for vitrinite reflectance
H_1	376 kJ/kg	The latent crystallization heat of magma
K_{host}		Thermal conductivity of host rocks
K_{magma}	2.1 J m^{-1} s^{-1}°C^{-1}	Thermal conductivity of the sill [*Galushkin*, 1997]
K_{matrix}	1.31 J m^{-1} s^{-1}°C^{-1}	Thermal conductivity of host rock matrix
K_{water}	0.6 J m^{-1} s^{-1}°C^{-1}	Thermal conductivity of water
L_d	170 kJ/kg	The latent heat of dehydration and decarbonation reactions of host rock matrix
P	Pa	The pressure of pore water
R		The ideal gas constant
t	second	Time
t_1		The final time of thermal evolution history
t_2		The time when magma intruded into host rocks
T	°C	Temperature
$T(t)$		The temperature at the time t
T_{d2}~T_{d1}	350~650°C	Temperature range of dehydration reactions of host rocks [*Galushkin*, 1997]
T_{c2}~T_{c1}	950~1150°C	Crystallization temperature range of melted magma [*Galushkin*, 1997]
ρ_{host}		Density of host rocks
ρ_{magma}	2700 kg/m^3	Density of the sill [*Galushkin*, 1997]
ρ_{matrix}	2700 kg/m^3	Density of host rock matrix
ρ_{water}		Density of pore water after intruding of magma
ρ_{water0}	1000 kg/m^3	Density of pore water before intruding of magma
α	0.001°C^{-1}	The thermal expansion coefficient of pore water
η	0.000133 Pa s	The dynamic viscosity of pore water
k		Permeability
φ	0.44	The porosity of host rocks [*Wang et al.*, 2011a, 2011b]
$\triangle t$	0.01 days	The time step
$\triangle Z$	0.3 m	The space step

heat of dehydration reactions in host rock matrix is considered in the model [*Galushkin*, 1997]. In this case, the source/sink term Q can be included [*Galushkin*, 1997].

$$Q = \frac{(1-\phi)\cdot\rho_{matrix}\cdot L_d}{T_{d1}-T_{d2}}\cdot\frac{\partial T}{\partial t} \quad . \tag{3}$$

When the temperature of the sill falls below the solidus of the magma, H_1 in equation (1) becomes zero. Fluid flow velocity can be computed from Darcy's law,

$$\mathbf{u} = -\frac{k}{\eta}\cdot(\nabla p - \rho_{water}\cdot\mathbf{g}) \tag{4}$$

and the continuity equation

$$\nabla\cdot(\rho_{water}\mathbf{u}) = 0. \tag{5}$$

The variation of pore water density with temperature is given by

$$\Delta\rho = -\alpha\cdot\rho_{water0}\cdot\Delta T \tag{6}$$

and the thermophysical properties of the host rocks can be computed from linear averaging

$$\rho_{host} = \rho_{matrix}\cdot(1-\phi) + \rho_{water}\cdot\phi \tag{7}$$

$$K_{host} = K_{matrix}\cdot(1-\phi) + K_{water}\cdot\phi \tag{8}$$

$$\text{Chost} = [\rho_{matrix}\cdot C_{matrix}\cdot(1-\phi) + \rho_{water}\cdot C_{water}\cdot\phi]/\rho_{host} \tag{9}$$

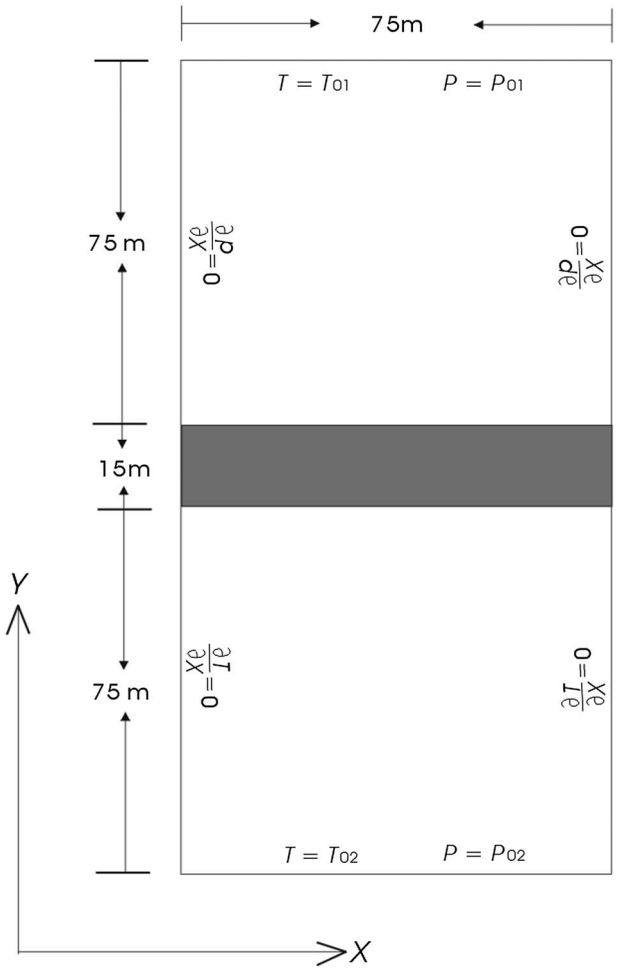

Figure 4. Model domain and boundary conditions.

3.2. Model Domain, Initial, and Boundary Conditions

The model domain and boundary conditions are shown in Figure 4. Because the abnormally high *R*r decreases to the background level at a distance of less than one sill thickness from the sill margins [*Peters et al.*, 1983; *Galushkin*, 1997], we specify upper and lower boundaries of the model 5 times the sill thickness away from sill margins [*Barker et al.*, 1998]. We also assume that two vertical boundaries are 5 times the sill thickness apart from each other. There is no inflow or outflow at these two vertical boundaries. Temperatures and pressures at the upper and lower boundaries are held constant.

The initial temperature of the host rocks (T_{host1}) is computed using a seafloor temperature of 5°C, a burial depth of 780 m, and a linear geothermal gradient of 75°C/km [*Galushkin*, 1997; *Wang et al.*, 2011a, 2011b]. The burial depth and the geothermal gradient are deduced from the reconstruction of burial-thermal history by *Galushkin* [1997]. According the porosity-burial depth relation of shales proposed by *Allen and Allen* [1990], the porosity of the host rocks when the sill intruded is approximately 0.44, slightly higher than the current porosity (~0.4). High porosity usually suggests high permeability. According to a simplified Kozeny-Carman equation describing the porosity-permeability relationship of shales [*Costa*, 2006; *Iyer et al.*, 2013], the permeability of the host rocks can be calculated to be about 30 md, with large uncertainties. Reasonable permeabilities are between 1/3 of and 3 times the computed value (i.e., 10 md $\leq k \leq$ 90 md). The upper end of this range is consistent with the permeability of unconsolidated organic-rich clay (e.g., layered and unweathered clay) which is generally below 100 md [*Bear*, 1972]. Thus, we consider permeabilities between 1 and 100 md, spanning the inferred range. All permeabilities exceed the threshold value (0.1 md) for the occurrence of hydrothermal convection in the host rocks [*Hayba and Ingebritsen*, 1997]. We allow the permeability of the sill to vary with temperature: the permeability of magma is 0.0019 md and that of the solidified magma is 0.19 md [*Dutrow et al.*, 2001]. The initial pressure of pore fluids is assumed to be hydrostatic. The thermophysical parameters of the sill and host rocks are listed in Table 1.

Table 2. Thermal History of Host Rocks Before Intruding of Magma[a]

Time (Myr)	Temperature (°C)	*R*o (%)
10	0	0.20
55	30	0.275
60	47	0.30
70	70	0.39

[a]All values from *Galushkin* [1997].

If magma is assumed to intrude the host rocks instantaneously, the prediction of the heat transfer models will largely overestimate thermal effects of the sill on the host rocks [*Galushkin*, 1997; *Wang et al.*, 2011a, 2011b]. Following *Galushkin* [1997], we allow the sill to intrude over a 6 h period with the center temperature increasing linearly from 100 to 1100°C in ~4.56 h.

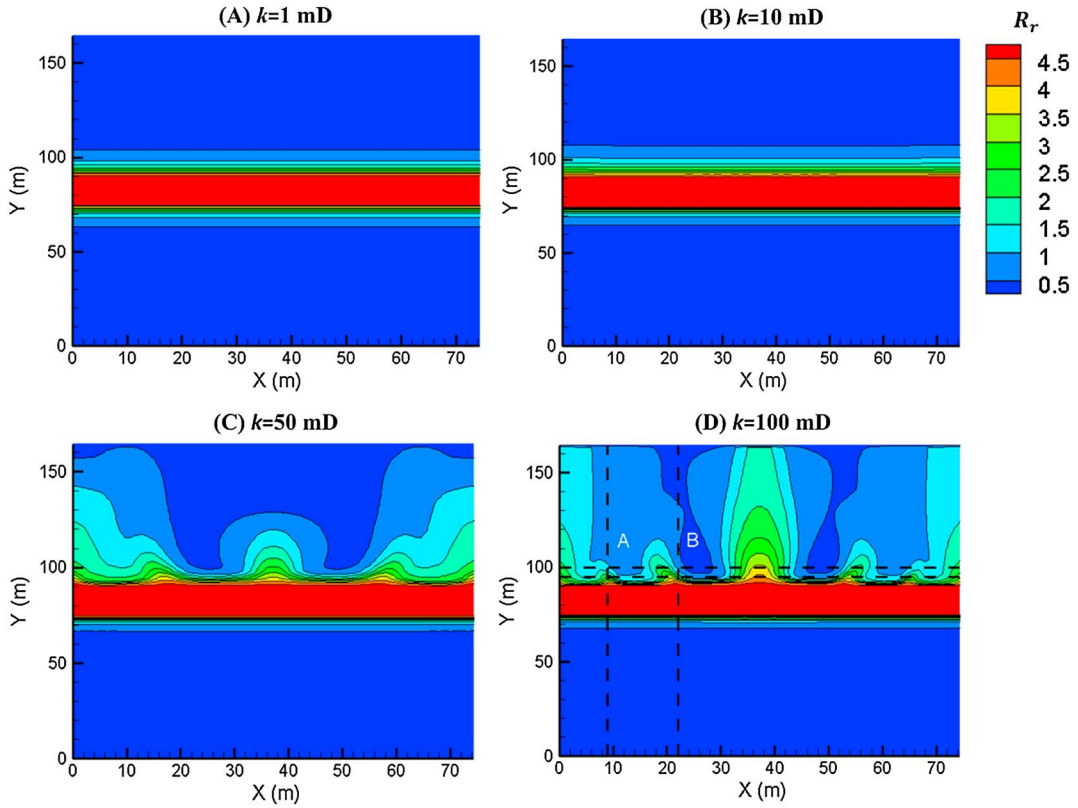

Figure 5. The computed spatial distribution of vitrinite reflectance for simulations with different permeabilities.

3.3. Model Outputs

Rr is a convenient index for evaluating organic matter maturation and can be computed based on the EASY% Ro model of *Sweeney and Burnham* [1990] and the thermal evolution history:

$$\text{EASY\%Ro} = \exp(3.7F - 1.6) \tag{10}$$

$$F = \sum_{i=1}^{20} f_i \cdot (1\text{-}C_i/C_{0i}) = \sum_{i=1}^{20} f_i \cdot (1\text{-}\exp(-I_i)) \tag{11}$$

$$I_i = \int_0^{t_1} A \cdot \exp(-E_i/(R \cdot T(t))) \cdot dt = \int_0^{t_2} A \cdot \exp(-E_i/(R \cdot T(t))) \cdot dt + \int_{t_2}^{t_1} A \cdot \exp(-E_i/(R \cdot T(t))) \cdot dt \tag{12}$$

The values of f_i, A, and E_i can be obtained from *Sweeney and Burnham* [1990]. I_i and F at any time during cooling of magma intrusions can be computed according to *Braun and Burnham* [1987]. The thermal evolution history of the host rocks during cooling of magma is obtained from the heat transfer model. The thermal evolution history of the host sediment before magma intrusion has been computed by *Galushkin* [1997] and is shown in Table 2. According to this thermal evolution history, the *Rr* background level before magma intrusion is evaluated to be approximately equal to 0.39%. Peak temperature (T_{peak}) is also an important parameter for studying thermal effects of igneous intrusions [*Barker et al.*, 1998; *Ogawa and Manga*, 2007]. We thus keep track of *Rr* and T_{peak} in order to compare model output to corresponding measurements.

4. Results and Discussion

4.1. Implications of Organic Matter Maturation Profiles

Figure 5 shows the computed spatial distribution of *Rr* in the model domain. Above the sill, the *Rr* isolines are almost horizontal for permeabilities of ≤10 md (Figures 5a and 5b), whereas the *Rr* varies significantly in the

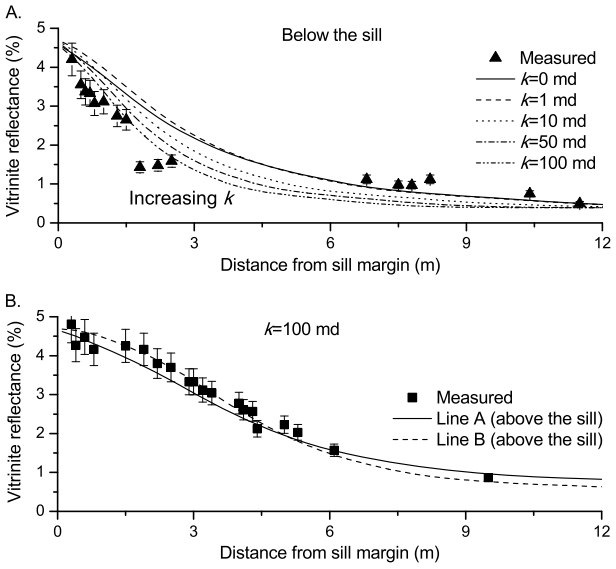

Figure 6. Comparison between the predicted vitrinite reflectance with the measured values. (a) Comparison between the predicted vitrinite reflectance for simulations with different permeabilities and measurements below the sill. (b) Comparison between the predicted vitrinite reflectance along the different vertical lines with the measured values above the sill. The locations of Lines A and B are shown in Figure 5d. Figures S1 and S2 in the supporting information show the effect of additional small sills.

horizontal direction for higher permeabilities (e.g., ≥30 md) (Figures 5c and 5d). Below the sill *R*r isolines are approximately horizontal in all cases. The spatial extent of the predicted abnormally high *R*r (>1.0%) is generally larger above the sill than below the sill when the permeability is >1 md, as observed in the measurements. Despite a different model setup and properties, *Iyer et al.* [2013] similarly reported high lateral variability of *R*r above the sill than below the sill when strong hydrothermal convection occurs.

Owing to the almost horizontal *R*r isolines below the sill, it is straightforward to make a robust comparison between the predicted *R*r and the measured values below the sill. As shown in Figure 6a, the computed *R*r (here we use the horizontally averaged value) decreases and gradually approaches the measured values with increased permeability. When the permeability reaches 100 md (the maximum reasonable permeability), the predicted *R*r profile matches well with the measurements. Importantly, for interpreting the measurements above the sill, we thus exclude the possibility of permeabilities smaller than several tens of millidarcies and of values we consider favor 100 md.

When the permeability is 100 md, we can compare the predicted *R*r with the measured values above the sill. From Figure 3, it can been seen that the *R*r of the underlying host rocks does not decline beyond 7 m from the sill and maintains a value of ~1.0%. Mature hydrocarbon assemblages produced by natural burial maturation are typically associated with source rocks with *R*r values from 0.45 to 1.0% [*Peters et al.*, 1983; *Galushkin*, 1997]. Thus, 1.0% approximately represents the current background level, and deposition and subsequent burial after magma intrusion has covered the thermal effect of the sill on the *R*r at these locations. As the *R*r decreases to ~1.0% at a distance of ~10 m above the sill, the *R*r should be ≤1.0% at this location during cooling of magma. In addition, the measured *R*r is observed to decrease to ~2.0% at a distance of ~5 m above the sill. Figure 5d shows that only the vertical *R*r profiles in the vicinity of Lines A and B can simultaneously match these observations. Figure 6b shows that the predicted *R*r profiles along both Lines A and B can match the overall measurements. However, with only one vertical profile of measurements, we cannot confirm whether either line is reasonable nor document the horizontal variability that is the hallmark of hydrothermal convection. In spite of a good match, more precisely constraining permeability is impractical because we cannot simply exclude the possibility of other permeabilities around 100 md. We can, however, at least infer that permeabilities are large enough to permit convection and that the measurements were made in a region with relatively weak upwelling.

The computed T_{peak} is shown in Figure 7. Similar to the spatial distribution of *R*r, T_{peak} isolines are almost horizontal below the sill, and T_{peak} varies in the horizontal direction above the sill. Thus, the obvious lateral variability in *R*r and T_{peak} above the sill record the occurrence of hydrothermal convection. However, the lack of the measured *R*r data parallel to the sill prohibits us from exploiting this features of the thermal evolution.

4.2. The Effects of Model Uncertainties

There are uncertainties in some model parameters and processes that need to be considered because if they result in overestimating, the effects of the sill on the *R*r of the underlying host rocks, the estimates of the

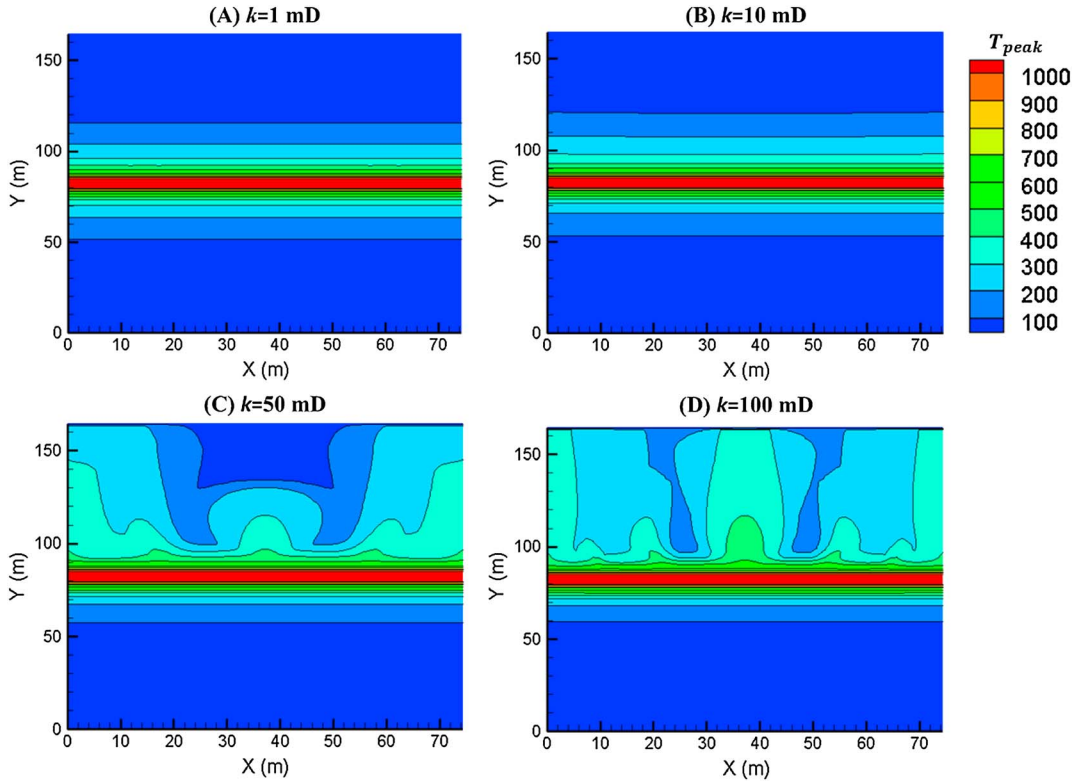

Figure 7. The spatial distribution of the computed peak temperature for simulations with different permeabilities.

permeability could be potentially biased. First, the uncertainties in some petrophysical parameters are a possible error source. A temperature of 1100°C is assumed to be the intrusion temperature of the sill based on its composition [*Hanson and Barton*, 1989; *Galushkin*, 1997]. *Wang* [2012] highlighted that the uncertainties in the intrusion temperature do not cause obvious deviation in the predicted *R*r. Further, 1100°C is a relatively low value for basaltic sills compared to the ones used by other workers (e.g., 1150°C and 1200°C) [*Santos et al.*, 2009; *Aarnes et al.*, 2010]. The relatively low intrusion temperature tends to decrease the spatial extent and degree of the thermal effect of the sill on the underlying host rocks. The instantaneous intrusion mechanism has been demonstrated to largely overestimate the thermal effects of the sill and thus can be simply excluded [*Galushkin*, 1997]. For the finite-time intrusion mechanism, we assumed a relatively thick precooled shell (~76% of the total sill thickness) for the sill, which lowers the total heat from the sill available for the underlying host rocks. Second, we specified the host rock temperature and the background maturation before sill emplacement based on the burial-thermal history performed by *Galushkin* [1997]. The uncertainties in these two parameters are small compared to other model parameters. The initial *R*r before magma emplacement is about 0.39%, whereas the current background *R*r lies in a range of 0.45%~1.0% [*Peters et al.*, 1983; *Galushkin*, 1997]. Even if we completely ignore the thermal effects of the subsequent burial (which last for about 19 Ma) after emplacement, the overestimation of the initial *R*r is ≤0.06% (0.45%–0.39% = 0.06%). The initial temperature of the host rocks is computed to be equal to ~65°C based on a high geothermal gradient (75°C/km). If the host rocks experienced a much lower background heat flow (30°C/km), the initial host rock temperature would become 30°C. The uncertainty is less than 35°C, even lower than the error in the intrusion temperature. In fact, the shallow sea depth together with geological evidence for magmatic activity in the area during basin development [*Van der Linden*, 1981; *Stillman et al.*, 1982; *Roussel and Linger*, 1983] indicate a high thermal regime of oceanic lithosphere, with high past and present-day heat flow [*Galushkin*, 1997]. Thus, the uncertainties in all of these parameters lead to small effects on *R*r and will not lead to an overestimate of the thermal effect of the sill on the underlying host rocks. It is worth emphasizing that the uncertainties in these parameters are not able to produce the asymmetric *R*r profiles above and below the sill.

In addition to the thermal buoyancy of pore water, other potential processes driving fluid flow also include fluid production from intruded magma and host rocks and virtual fluid production from deformation. The degree of the effects of the fluid production from both the magma and host rocks on fluid pressure and fluid flow depends on porosity, permeability, and the amount of produced fluids [*Hanson*, 1995]. Following *Jamtveit et al.* [2004], a dimensionless parameter *Ve* will characterize the importance of these additional sources, scaling inversely with the total burial depth (i.e., the water depth of 3367 m plus 780 m bsl emplacement depth) and the permeability [see also *Ingebritsen et al.*, 2006]. For the 15 m thick sill, *Ve* is generally less than 1.0 for the pure water case (no boiling), implying that fluid pressure decays rapidly and corresponds to the situation where pressure diffusion is fast compared to the rate of pressure production, limiting significant fluid pressure buildup. *Hanson* [1995] similarly noted that for typical water contents of magmas (the completely melted magma) and host rocks, permeabilities of $\leq$1 μd are required to effectively increase pore fluid pressure and obviously influence fluid flow. This permeability threshold is much lower than the assumed values for the host rocks. Furthermore, our model specifies a finite-time intrusion for the sill and assumes a precooled solid shell (>50% of the total thickness of the sill). Thus, the fluid production from the magma is decreased compared to instantaneously intruded thick sills (100 m~10 km) [*Hanson*, 1995; *Iyer et al.*, 2013]. Further, dehydration reactions of the host rocks are restricted by a regime of increasing rock temperature and to a temperature interval between T = 350~650°C [*Walther and Orville*, 1982; *Walther and Woud*, 1984; *Hanson and Barton*, 1989]. Figure 7 shows that for most regions near the sill, T_{peak} is below 500°C, which means that less than half of the water in mineral assemblages is released during contact metamorphism. The narrow spatial extent available for the dehydration reactions ($T_{peak} > 350$°C) and the low degree of dehydration reactions also limit the contribution of the released water by the dehydration reactions to pressure buildup and fluid flow. Although we have neglected fluid production because we expect it to be insignificant, the effects of thermal pressurization and fluid production may need to be included to compare models and measurements in other cases.

In the zones where we see effects of the sill on *R*r, the host rocks are mainly composed of shales. Because of the moderate sill thickness (15 m), the difference in the initial organic maturation and the petrophysical properties above and below the sill are small and, hence, are ignored. However, the lithology log of the studied section (Figure 1) shows two thin sills, with thickness of 20~30 cm, located above the larger 15 m thick sill. Given their thickness, the total heat of a small sill only accounts for 1.3~2.0% of the larger one; thus, the effects of these two small sills were ignored in our (and others') models [e.g., *Peters et al.*, 1978; *Galushkin*, 1997]. We also tested the effect of a thin sill above the larger sill on the overall maturation distribution. Results are included in Text S1 and Figures S1 and S2 in the supporting information. The simulation results show that the small sills do not influence the overall maturation distribution.

5. Conclusions

Based on comparing the heat convection model with measurements in the contact aureole of a 15 m thick sill intrusion, we draw the following conclusions:

1. Below the sill, the computed *R*r and T_{peak} isolines are approximately horizontal for all permeabilities. Above the sill, for high permeabilities (e.g., $\geq$50 md), the computed *R*r and T_{peak} isolines will fluctuate significantly parallel to the sill. The high lateral variability in *R*r above a horizontal sill could be regarded as potential evidence for assessing whether thermal convection of pore water occurred in host rocks. Although we cannot determine where the *R*r measurements were made relative to the location of upwellings and downwellings, we can, however, at least infer that the measurements were made in a region with relatively weak upwelling.
2. According to measurements, the spatial extent of the abnormally high *R*r is larger above the sill than below the sill. This pattern cannot be explained by heat conduction alone. Instead, thermal convection in a host rock with permeability of approximately tens of millidarcies can reproduce the observed pattern.

Acknowledgments
Authors acknowledge Henrik Svensen and Ingrid Aarnes for their constructive comments, which greatly improve the clarity of our manuscript. This work was financially supported by the National Science Foundation of China (51376033 and 41004031) and the Fundamental Research Funds for the Central Universities (DUT15LAB18) with additional support for Michael Manga from the U.S. National Science Foundation. The data used in this manuscript are available for free. The authors acknowledge and comply with AGU's data policy.

References

Aarnes, I., H. Svensen, J. A. D. Connolly, and Y. Y. Podladchikov (2010), How contact metamorphism can trigger global climate changes: Modeling gas generation around igneous sills in sedimentary basins, *Geochim. Cosmochim. Acta*, *74*(24), 7179–7195.

Aarnes, I., H. Svensen, S. Polteau, and S. Planke (2011), Contact metamorphic devolatilization of shales in the Karoo Basin, South Africa, and the effects of multiple sill intrusions, *Chem. Geol.*, *281*(3–4), 181–194.

Allen, P. A., and J. R. Allen (1990), *Basin Analysis: Principles and Applications*, pp. 463, Blackwell Scientific Pub., Oxford.
Barker, C. E. (1996), A comparison of vitrinite reflectance measurements made on whole-rock and dispersed organic matter concentrate mounts, *Org. Geochem.*, *24*, 251–256.
Barker, C. E., Y. Boney, and M. D. Lewan (1998), Fluid inclusion and vitrinite-reflectance geothermometry compared to heat-flow models of maximum paleotemperature next to dikes, western onshore Gippsland Basin, Australia, *Int. J. Coal Geol.*, *37*, 73–111.
Bear, J. (1972), *Dynamics of Fluids in Porous Media*, Dover Pub., New York.
Bishop, A. N., and C. D. Abbott (1995), Vitrinite reflectance and molecular geochemistry of Jurassic sediments: The influence of heating by Tertiary dyke (northwest Scotland), *Org. Geochem.*, *22*, 165–177.
Bostick, N. H., and M. J. Pawlewicz (1984), Paleotemperatures based on vitrinite reflectance of shales and limestones in igneous dike aureoles in the upper cretaceous Pierre shale, Walsenburg, Colorado, in *Hydrocarbon Source Rocks of the Greater Rocky Mountain Region*, edited by J. Woodward, F. F. Meisner, and J. L. Clayton, pp. 387–392, Rocky Mountain Association of Geologists, Denver, Colo.
Braun, R. L., and A. K. Burnham (1987), Analysis of chemical reaction kinetics using a distribution of activation energies and simpler models, *Energy Fuels*, *1*(2), 153–161.
Cao, X., M. Chappell, A. Schimmelmann, M. Mastalerz, Y. Li, W. Hu, and J. Mao (2013), Chemical structure changes in kerogen from bituminous coal in response to dike intrusions as investigated by advanced solid-state ^{13}C NMR spectroscopy, *Int. J. Coal Geol.*, *108*, 53–64.
Costa, A. (2006), Permeability-porosity relationship: A reexamination of the Kozeny-Carman equation based on a fractal pore-space geometry assumption, *Geophys. Res. Lett.*, *33*, L02318, doi:10.1029/2005GL025134.
Delaney, P. T. (1982), Rapid intrusion of magma into wet rocks: Groundwater flow due to pore pressure increases, *J. Geophys. Res.*, *87*, 7739–7756, doi:10.1029/JB087iB09p07739.
Dutrow, B. L., B. J. Travis, B. J. Gable, and D. J. Henry (2001), Coupled heat and silica transport associated with dike intrusion into sedimentary rock: Effects on isotherm location and permeability evolution, *Geochim. Cosmochim. Acta*, *65*(21), 3749–3767.
Fjeldskaar, W., H. M. Helset, H. Johansen, I. Grunnaleite, and I. Horstad (2008), Thermal modeling of magmatic intrusions in the Gjallar Ridge, Norwegian Sea: Implications for vitrinite reflectance and hydrocarbon maturation, *Basin Res.*, *20*, 143–159.
Fu, F. Q., B. I. A. McInnes, N. J. Evans, and P. J. Davies (2010), Numerical modeling of magmatic-hydrothermal systems constrained by U–Th–Pb–He time–temperature histories, *J. Geochem. Explor.*, *106*, 90–109.
Galushkin, Y. I. (1997), Thermal effects of igneous intrusions on maturity of organic matter: A possible mechanism of intrusion, *Org. Geochem.*, *26*(11–12), 645–658.
Hanson, R. B. (1995), The hydrodynamics of contact metamorphism, *GSA Bull.*, *107*(5), 595–611.
Hanson, R. B., and M. D. Barton (1989), Thermal developmentof low-pressure metamorphic belts: Results from two-dimensional numerical models, *J. Geophys. Res.*, *94*(B8), 10,363–10,377, doi:10.1029/JB094iB08p10363.
Hayba, D. O., and S. E. Ingebritsen (1997), Multiphase groundwater flow near cooling plutons, *J. Geophys. Res.*, *102*, 12,235–12,252, doi:10.1029/97JB00552.
Ingebritsen, S. E., W. E. Sanford, and C. Neuzil (2006), *Groundwater in Geologic Processes*, 2nd ed., Cambridge Univ, Press.
Iyer, K., L. Rüpke, and Y. Galerne (2013), Modeling fluid flow in sedimentary basins with sill intrusions: Implications for hydrothermal venting and climate change, *Geochem. Geophys. Geosyst.*, *14*, 5244–5262, doi:10.1002/2013GC005012.
Jaeger, J. C. (1959), Temperatures outside a cooling intrusive sheet, *Am. J. Sci.*, *257*, 44–54.
Jamtveit, B., H. Svensen, Y. Y. Podladchikov, and S. Planke (2004), Hydrothermal vent complexes associated with sill intrusions in sedimentary basins, in *Physical Geology of High-Level Magmatic Systems*, edited by C. Breitkreuz and N. Petford, pp. 233–241, Geol. Soc., Bath.
Jones, F., H. Wielens, M. C. Williamson, and M. Zentilli (2007), Impact of magmatism on petroleum systems in the Sverdrup Basin, anadian Arctic Islands, Nunavut: A numerical modeling study, *J. Petrol. Geol.*, *30*(3), 237–255.
Lancelot, Y., and E. Seibold (1977), Initial reports of the Deep Sea Drilling Project, vol. 41, pp. 1259, U.S. Gov. Print. Off., Washington, D. C.
Mastalerz, M., A. Drobniak, and A. Schimmelmann (2009), Changes in optical properties, chemistry, and micropore and mesopore characteristics of bituminous coal at the contact with dikes in the Illinois Basin, *Int. J. Coal Geol.*, *77*, 310–319.
Norton, D. L., and J. B. Hulen (2001), Preliminary numerical analysis of the magma-hydrothermal history of the Geysers geothermal system, California, USA, *Geothermics*, *30*, 211–234.
Ogawa, Y., and M. Manga (2007), Thermal demagnetization of Martian upper crust by magma intrusion, *Geophys. Res. Lett.*, *34*, L16302, doi:10.1029/2007GL030565.
Othman, R., K. R. Arouri, C. R. Ward, and D. McKirdy (2001), Oil generation by igneous intrusions in the northern Gunnedah Basin, Australia, *Org. Geochem.*, *32*, 1219–1232.
Peters, K. E., B. R. T. Simoneit, S. Brenner, and I. R. Kaplan (1978), Vitrinite reflectance-temperature determinations for intruded Cretaceous black shale in the eastern Atlantic, in *Symposium in Geochemistry: Low Temperature Metamorphism of Kerogen and Clay Minerals*, edited by D. Otz, pp. 53–58, SEPM Pacific Section, Los Angelos, Calif.
Peters, K. E., J. K. Whelan, J. M. Hunt, and H. F. Tarafa (1983), Programmed pyrolysis of organic matter from thermally altered Cretaceous black shales, *AAPG Bull.*, *67*(11), 2137–2149.
Roussel, J., and J. L. Linger (1983), A review of deep structure and ocean-continent transition in the Senegal basin (West Africa), *Tectonophysics*, *91*, 183–211.
Santos, R. V., E. L. Dantas, C. G. de Oliveira, C. J. de Alvarenga, C. W. dos Anjos, E. M. Guimaraes, and F. B. Oliveira (2009), Geochemical and thermal effects of a basic sill on black shales and limestones of the Permian Irati Formation, *J. S. Am. Earth Sci.*, *28*(1), 14–24.
Schimmelmann, A., M. Mastalerz, L. Gao, P. E. Sauer, and K. Topalov (2009), Dike intrusions into bituminous coal, Illinois Basin: H, C, N, O isotopic responses to rapid and brief heating, *Geochim. Cosmochim. Acta*, *73*(20), 6264–6281.
Simoneit, B. R. T., S. Brenner, K. E. Peters, and I. R. Kaplan (1978), Thermal alteration of Cretaceous black shale by basaltic intrusions in the eastern Atlantic, *Nature*, *273*, 501–504.
Simoneit, B. R. T., S. Brenner, K. E. Peters, and I. R. Kaplan (1981), Thermal alteration of Cretaceous black shale by diabase intrusions in the eastern Atlantic. Part II. Effects on bitumen and kerogen, *Geochim. Cosmochim. Acta*, *45*(9), 1581–1602.
Stewart, A. K., M. Massey, P. L. Padgett, S. M. Rimmer, and J. C. Hower (2005), Influence of a basic intrusion on the vitrinite reflectance and chemistry of the Springfield (No. 5) coal, Harrisburg, Illinois, *Int. J. Coal Geol.*, *63*, 58–67.
Stillman, C. J., H. Furnes, M. J. LeBas, A. H. F. Robertson, and J. Zielonka (1982), The geological history of Maio, Cape Verde Islands, *J. Geol. Soc. London*, *139*, 347–361.
Sweeney, J. J., and A. K. Burnham (1990), Evaluation of a simple model of vitrinite reflectance based on chemical kinetics, *AAPG Bull.*, *74*, 1559–1570.
Turcotte, D. L., and G. Schubert (1982), *Geodynamics Applications of Continuum Physics to Geological Problems*, Wiley, New York.

Valentim, B., A. Guedes, S. Rodrigues, and D. Flores (2011), Case study of igneous intrusion effects on coal nitrogen functionalities, *Int. J. Coal Geol.*, *86*, 291–294.

Van der Linden, W. I. M. (1981), The crustal structure and evolution of the continental margin off Senegal and Gambia, from total-intensity magnetic anomalies, *Geol. Mijnbouw*, *60*(2), 257–266.

Vasquez, M., U. Altenberger, and R. L. Romer (2009), Neogene magmatism and its possible causal relationship with hydrocarbon generation in SW Colombia, *Int. J. Earth Sci.*, *98*(5), 1053–1062.

Walther, J. V., and B. J. Woud (1984), Rate and mechanism in prograde metamorphism, *Contrib. Mineral. Petrol.*, *88*(3), 246–259.

Walther, J. V., and P. M. Orville (1982), Volatile production and transport in regional metamorphism, *Contrib. Mineral. Petrol.*, *79*(3), 252–257.

Wang, D. (2012), Comparable study on the effect of errors and uncertainties of heat transfer models on quantitative evaluation of thermal alteration in contact metamorphic aureoles: Thermophysical parameters, intrusion mechanism, pore water volatilization and mathematical equations, *Int. J. Coal Geol.*, *95*, 12–19.

Wang, D. (2013), MagmaHeatNS1D: One-dimensional visualization numerical simulator for computing thermal evolution in a contact metamorphic aureole, *Comput. Geosci.*, *54*, 21–27.

Wang, D., and Y. Song (2012), Influence of different boiling points of pore water around an igneous sill on the thermal evolution of the contact aureole, *Int. J. Coal Geol.*, *104*, 1–8.

Wang, D., X. Lu, X. Zhang, S. Xu, W. Hu, and L. Wang (2007), Heat-model analysis of wall rocks below a diabase sill in Huimin Sag, China compared with thermal alteration of mudstone to carbargilite and hornfels and with increase of vitrinite reflectance, *Geophys. Res. Lett.*, *34*, L16312, doi:10.1029/2007GL030314.

Wang, D., X. Lu, S. Xu, and W. Hu (2008), Influence of a basic intrusion on the vitrinite reflectance and chemistry of the Springfield (No. 5) coal, Harrisburg, Illinois, *Int. J. Coal Geol.*, *73*, 196–199.

Wang, D., X. Lu, Y. Song, R. Shao, and T. Qi (2010), Influence of the temperature dependence of thermal parameters of heat conduction models on the reconstruction of thermal history of igneous-intrusion-bearing basins, *Comput. Geosci.*, *36*, 1339–1344.

Wang, D., Y. Song, W. Liu, M. Zhao, and T. Qi (2011a), Numerical investigation of the effect of volatilization and the supercritical state of pore water on maturation of organic matter in the vicinity of igneous intrusions, *Int. J. Coal Geol.*, *87*, 33–40.

Wang, D., Y. Song, H. Xu, X. Ma, and M. Zhao (2013), Numerical modeling of thermal evolution in the contact aureole of a 0.9 m thick dolerite dike in the Jurassic siltstone section from Isle of Skye, Scotland, *J. Appl. Geophys.*, *89*, 134–140.

Wang, K., X. Lu, M. Chen, Y. Ma, K. Liu, L. Liu, X. Li, and W. Hu (2011b), Numerical modelling of the hydrocarbon generation of Tertiary source rocks intruded by doleritic sills in the Zhanhua depression, Bohai Bay Basin, China, *Basin Res.*, *23*, 1–14.